Journal of Heat and Mass Transfer Research 7 (2020) 95- 103

Journal of Heat and Mass Transfer Research

Journal homepage: http://jhmtr.semnan.ac.ir

Semnan University

Unsteady Coupled Heat and Mass Transfer by Free Convection from a Vertical Plate Embedded in Porous Media under Impacts of Radiation and Chemical Reaction

A. M. Aly [*,a,b], A. J. Chamkha [c], Z. A. S. Raizah [a]

[a]Department of Mathematics, Faculty of Science, Abha, King Khalid University, Saudi Arabia.
[b]Department of Mathematics, Faculty of Science, South Valley University, Qena, Egypt.
[c] Faculty of Engineering, Kuwait College of Science and Technology, Doha District, Kuwait.

PAPER INFO

Paper history:
Received: 2017-03-06
Revised: 2019-07-19
Accepted: 2019-07-23

Keywords:
Finite-difference solution;
Radiation;
Chemical reaction;
Porous medium.

ABSTRACT

This research presented numerical solution for the unsteady natural convection of coupled heat and mass transfer over a vertical plate embedded in a uniform porous medium. Here, the impacts of the thermal radiation and chemical reaction were considered. An explicit finite-difference scheme is used to solve the governing equations. The radiative heat flux was expressed by Roseland approximation in the energy equation. The solutions at each iteration have been obtained to reach the steady state. The graphical form of numerical results is introduced to present the effects of material parameters on the solution. It is found that, the skin-friction coefficient increased as either of the thermal buoyancy, solutal buoyancy, Reynolds number or the inverse thermal radiation parameter increased. The Nusselt number increases due to increases in Prandtl number, thermal buoyancy, solutal buoyancy and Reynold number while it decreases as the permeability parameter, inverse thermal radiation parameter, chemical reaction parameter and the Schmidt number are increase.

DOI: 10.22075/jhmtr.2019.10763.1149

1. Introduction

The impacts of the chemical reaction on heat and mass transfer problems are of importance in several processes such as drying, evaporation at the surface of a water body and the flow in a desert cooler. Also, applications of this type of flow can be found in many industries, geophysics and engineering. For this reason, it has received a considerable amount of attention in recent years. Chemical reactions can be defined as either heterogeneous or homogeneous processes. The problem of unsteady free convection flow over a vertical plate has been studied previously by such authors as Gokhale [1], Takhar et al. [2] and Muthukumaraswamy and Ganesan [3]. Takhar et al. [4] studied the influences of thermal radiation on MHD flow of a gas past a semi-infinite vertical plate.

Muthucumaraswamy and Ganesan [5] have considered the impacts of diffusion and chemical reaction on impulsively-started infinite vertical plate. Anjali Devi and Kandasamy [6] considered the impacts of chemical reaction on non-linear MHD boundary-layer flow over a wedge. Sieniutycz [7] studied chemical or electrochemical reactions. Dogan et al. [8] reported numerically the heat and mass transfer in a metal hydride bed. Kandasamy et al. [9] depicted the heat source and concentration on a wedge with suction or injection. Kandasamy et al. [10] considered chemical reaction effects on MHD flow over a vertical stretching surface. In addition, Chamkha and his co-authors (Chamkha et al. [11], Chamkha et al. [12], Chamkha et al. [13] and Chamkha and Aly [14]), introduced several problems related to the impacts of the chemical reaction on heat and mass transfer in a boundary layer flow though vertical plates with different conditions. Mansour et al. [15] used a fourth order Runge-Kutta scheme with the shooting method to analysis the effects of chemical reaction and Soret number and Dufour number on MHD free convection on a vertical stretching surface.

[*]Corresponding Author: A. M. Aly, Department of Mathematics, Faculty of Science, Abha, King Khalid University, Saudi Arabia.
Email: abdelreheam.abdallah@sci.svu.edu.eg

There are numerous studies related to the impacts of the radiation on MHD boundary layer flow past a vertical plate (Abd El-Naby et al. [16], Ganesan and Palani [17], EL-Kabeir et al. [18], Mbeledogu and Ogulu [19], Rashad et al. [20], Basiri et al. [21])

The main objective of this work is to analysis the unsteady natural convection from a vertical plate in a uniform porous medium under influences of thermal radiation and chemical reaction. The governing equations are solved using an explicit finite-difference scheme. The Roseland approximation is used to describe the radiative heat flux in the energy equation. The impact of the material parameters on the current problem are represented in graphical form.

2. Mathematical Analysis

Consider unsteady, laminar, boundary layer, two-dimensional free convective flow over a vertical flat plate in a uniform porous medium under influences of thermal radiation effects. The governing boundary-layer equations are:

$$\frac{\partial \bar{u}}{\partial \bar{x}} + \frac{\partial \bar{v}}{\partial \bar{y}} = 0 \tag{1}$$

$$\frac{\partial \bar{u}}{\partial \bar{t}} + \bar{u}\frac{\partial \bar{u}}{\partial \bar{x}} + v\frac{\partial \bar{u}}{\partial \bar{y}} = \nu\,\frac{\partial^2 \bar{u}}{\partial \bar{y}^2} + g\beta_T\left(\overline{T} - \overline{T_\infty}\right) + g\beta_C\left(\overline{C} - \overline{C_\infty}\right) - \frac{\nu}{k_1}\bar{u} \tag{2}$$

$$\frac{\partial \bar{T}}{\partial \bar{t}} + \bar{u}\frac{\partial \bar{T}}{\partial \bar{x}} + \bar{v}\frac{\partial \bar{T}}{\partial \bar{y}} = \frac{k}{\rho C_p}\frac{\partial^2 \bar{T}}{\partial \bar{y}^2} - \frac{1}{\rho\, C_P}\frac{\partial q_r}{\partial \bar{y}} \tag{3}$$

$$\frac{\partial \bar{C}}{\partial \bar{t}} + \bar{u}\frac{\partial \bar{C}}{\partial \bar{x}} + \bar{v}\frac{\partial \bar{C}}{\partial \bar{y}} = D\frac{\partial^2 \bar{C}}{\partial \bar{y}^2} - k_c(\bar{C} - \bar{C}_\infty) \tag{4}$$

It is simplified by using the Rosseland approximation (see Sparrow and Cess [15]) as

$$q_r = -\frac{4\sigma_0}{3k^*}\frac{\partial \bar{T}^4}{\partial \bar{y}} \tag{5}$$

where σ_0 and k^* are the Stefan-Boltzman constant and the mean absorption coefficient, respectively. The Taylor series expansion for $\bar{T}^4$neglecting higher order terms is:

$$\bar{T}^4 = 4\,\bar{T}_\infty^3\bar{T} - 3\bar{T}_\infty^4 \tag{6}$$

Substitution of Equations (5) and (6) in the energy equation (3), one obtains:

$$\frac{\partial \bar{T}}{\partial \bar{t}} + \bar{u}\frac{\partial \bar{T}}{\partial \bar{x}} + \bar{v}\frac{\partial \bar{T}}{\partial \bar{y}} = \frac{k}{\rho C_p}\left(1 + \frac{4}{3R}\right)\frac{\partial^2 \bar{T}}{\partial \bar{y}^2} \tag{7}$$

The boundary conditions are:

$$\begin{aligned}
&\bar{t} = 0: \quad \bar{u} = \bar{v} = 0,\ \bar{T} = \bar{T}_\infty, \bar{C} = \bar{C}_\infty \\
&\text{ for all } \bar{x} \text{ and } \bar{y} \\
&\bar{t} > 0: \\
&\bar{u} = \bar{v} = 0, \bar{T} = \bar{T}_\infty, \bar{C} = \bar{C}_\infty \quad at\ \bar{x} = 0 \\
&\bar{u} = \bar{v} = 0, \bar{T} = \bar{T}_W, \bar{C} = \bar{C}_W \quad at\ \bar{y} = 0, \bar{x} > 0 \\
&\bar{u} = 0, \bar{T} = \bar{T}_\infty, \bar{C} = \bar{C}_\infty \qquad at\ \bar{y} \to \infty, \bar{x} > 0
\end{aligned} \tag{8}$$

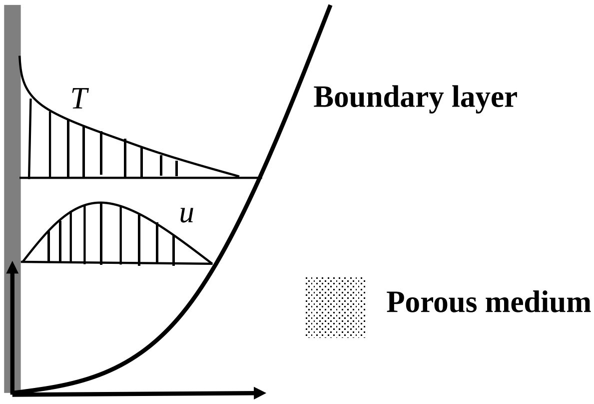

Figure1. Initial physical model.

where $\overline{T}_W$ and $\overline{C}_W$ are the wall temperature and concentration. The physical model governing on this problem is presented in figure 1.

The dimensionless variables are:

$$x = \frac{\bar{x}}{l}, y = \frac{\bar{y}}{l},\ u = \frac{\bar{u}}{U}, v = \frac{\bar{v}}{U},\ T = \frac{\bar{T} - \bar{T}_\infty}{\bar{T}_W - \bar{T}_\infty}, C = \frac{\bar{C} - \bar{C}_\infty}{\bar{C}_W - \bar{C}_\infty}, t = \frac{U\,\bar{t}}{l} \tag{9}$$

Substituting Equations (9) into Equations (1), (2), (4) and (7)-(9) gives the following dimensionless equations:

$$\frac{\partial u}{\partial x} + \frac{\partial v}{\partial y} = 0 \tag{10}$$

$$\frac{\partial u}{\partial t} + u\frac{\partial u}{\partial x} + v\frac{\partial u}{\partial y} = \frac{1}{\mathrm{Re}}\frac{\partial^2 u}{\partial y^2} + Gr\,T + Gc\,C - \frac{K}{\mathrm{Re}}\,u \tag{11}$$

$$\frac{\partial T}{\partial t} + u\frac{\partial T}{\partial x} + v\frac{\partial T}{\partial y} = \frac{1}{\mathrm{Re\ Pr}}\left(1 + \frac{4}{3\,R}\right)\frac{\partial^2 T}{\partial y^2} \tag{12}$$

$$\frac{\partial C}{\partial t} + u\frac{\partial C}{\partial x} + v\frac{\partial C}{\partial y} = \frac{1}{Sc\ \mathrm{Re}}\frac{\partial^2 C}{\partial y^2} - \gamma\,C \tag{13}$$

where $\mathrm{Re} = \frac{U\,l}{\nu}$ is the Reynold's number, $K = \frac{l^2}{k_1}$is the non-dimensional permeability parameter, $Gr = \frac{g\,\beta_T(T_W - T_\infty)\,l}{U^2}$, is Grashof number and $Gc = \frac{g\,\beta_C(C_W - C_\infty)\,l}{U^2}$ is the modified Grashof number, $Sc = \frac{\nu}{D}$is the Schmidt number,$\mathrm{Pr} = \frac{\rho \nu C_P}{k}$ is the Prandtl number, $R = \frac{k\,k^*}{4\,\sigma_0\,T_\infty^3}$is the radiation parameter, and $\gamma = \frac{k_c l}{U}$ is the chemical reaction parameter.

The dimensionless boundary conditions are:

$$\begin{aligned}
&t = 0: \quad u = v = 0,\ T = C = 0\ \text{ for all } x \text{and } y \\
&t > 0: \\
&u = v = 0, T = C = 0 \qquad at\ x = 0 \\
&u = v = 0, T = C = 1 \qquad at\ y = 0, x > 0 \\
&u = 0, T = C = 0 \qquad\quad at\ y \to \infty, x > 0
\end{aligned} \tag{14}$$

This type of flow, heat and mass transfer situation have special significance such as the skin-friction coefficientC_f, the Nusselt number Nuand the Sherwood number *Sh*. These physical quantities are defined in dimensionless form, respectively, as follows:

$$\mathrm{C_f}\ \mathrm{Re}^{\frac{1}{2}} = \mathrm{u}'(t, \mathrm{x}, 0) \tag{15}$$

$$Nu\ Re^{-\frac{1}{2}} = -T'\ (t, x, 0) \tag{16}$$

$$Sh\ Re^{-\frac{1}{2}} = -C'\ (t, x, 0) \tag{17}$$

3. Solution Technique

The non-linear equations (10)-(13) with boundary conditions (14) are solved by an explicit finite-difference scheme. The length of the plate is units and the thickness of boundary-layer is At the end of time step and are the values of and . The approximate set of the finite-difference equations corresponding to Equations (10)-(13) are:

$$\frac{u'_{i,j} - u'_{i-1,j}}{\Delta x} + \frac{v'_{i,j+1} - v'_{i,j}}{\Delta y} = 0 \tag{18}$$

$$\frac{u'_{i,j} - u_{i,j}}{\Delta t} + u_{i,j}\frac{u_{i,j} - u_{i-1,j}}{\Delta x} + v_{i,j}\frac{u_{i,j+1} - u_{i,j}}{\Delta y} = \frac{1}{\mathrm{Re}}\left(\frac{u_{i,j+1} - 2u_{i,j} + u_{i,j-1}}{(\Delta y)^2}\right) + Gr\,T'_{i,j}\ Gc\,C'_{i,j} - \frac{K}{\mathrm{Re}}\,u_{i,j} \tag{19}$$

$$\frac{T'_{i,j} - T_{i,j}}{\Delta t} + u_{i,j}\frac{T_{i,j} - T_{i-1,j}}{\Delta x} + v_{i,j}\frac{T_{i,j+1} - T_{i,j}}{\Delta y} = \frac{1}{Pr\ Re}\left(1 + \frac{4}{3\ R}\right)\left(\frac{T_{i,j+1} - 2T_{i,j} + T_{i,j-1}}{(\Delta y)^2}\right) \tag{20}$$

$$\frac{C'_{i,j} - C_{i,j}}{\Delta t} + u_{i,j}\frac{C_{i,j} - C_{i-1,j}}{\Delta x} + v_{i,j}\frac{C_{i,j+1} - C_{i,j}}{\Delta y} = \frac{1}{Sc\ \mathrm{Re}}\left(\frac{C_{i,j+1} - 2C_{i,j} + C_{i,j-1}}{(\Delta y)^2}\right) - \gamma C'_{i,j} \tag{21}$$

where (i, j) represents the grid points. The final steady state solution is obtained for which both $\partial u/\partial t, \partial T/\partial t$ and $\partial C/\partial t$are zero. The coefficients $u_{i,j}$ and $v_{i,j}$ are constants during any one time-step.

At various dimensionless times, the velocity, temperature and concentration profiles were calculated. The region of integration is considered as a rectangle with sides x_{max} (10) and y_{max} (30). After few tests on mesh sizes to reach the grid independence, the time and spatial step sizes Δt = 0.05, Δx =0.1 and Δy =0.25 were found to give accurate results. The complete results for $t = 10, 20, \ldots 80$ show slight changes in $u, v, T$and$C$. The value $t = 80$ is used in most of the figures (Pr=0.71) and is considered as representing the steady-state condition. The validations of the current explicit finite-difference scheme were performed several times during our previous studies (Chamkha et al. [22, 23] and Aly and Ahmed [24]). Figure 2 shows an accuracy tests at three sets of grids: 30×30, 40×40, 50×50. It is clear that 40×40 uniform grid is found to meet the requirements of both the grid independence study and the computational time limits.

4. Results and Discussion

In this section, a set of graphical results at x=10 is presented in figures 3-11. These figures illustrate the impact of the permeability parameter K, the chemical reaction parameter γ, the Prandtl number Pr, the Schmidt number Sc, the radiation parameter R, and the dimensionless time of flow process on the velocity, temperature and the concentration profiles. The temporal or time-dependent results are shown in figures 12-19.

Figures 3-5 present the impact of the variations on permeability parameter K in the typical velocity, temperature and concentration profiles. An extra value of K has the tendency to resist the flow causing its velocity to decrease while its temperature and concentration species to increase. This happens with little changes in the thicknesses of the momentum, thermal and concentration boundary layers. For the parametric conditions, it is observed that the changes in the velocity and temperature profiles are more pronounced than those of the concentration profiles as the permeability parameter increases. All of these behaviors are clearly observed in figures 3-5.

Figures 6 and 7 display the impacts of the thermal radiation parameter R on the velocity and the temperature profiles. Decreasing the thermal radiation parameter R makes important increase in the thermal state of the fluid causing its temperature to increase. The virtue of the thermal buoyancy effect causes an in increase in the fluid temperature causing the velocity of the fluid there to increase. These trends are clearly depicted by the increases in the velocity and temperature profiles as R decreases shown in figures 6 and 7.

The impacts of the chemical reaction parameter γ on the velocity and concentration profiles have been depicted in figures 8 and 9. An increase on chemical reaction parameter causes a decrease in the species concentration. This causes the concentration buoyancy influences to decrease as γ increases. Consequently, less flow is induced along the plate resulting a decrease on fluid velocity in the boundary layer. In addition, the concentration boundary layer thickness decreases as γ increases. These behaviors are seen in figures 8 and 9.

Figure 10 presents the temperature profiles under variations of the Prandtl number Pr. It is well known that the Prandtl number is presented by the ratio between the thicknesses of the viscous and thermal boundary layers. An increase on Pr causes the fluid temperature to decrease and the thermal boundary layer thickness to shrink significantly as seen from figure 10.

The effects of increasing the Schmidt number Sc on the concentration profiles are shown in figure 11. The Schmidt number is considering a factor in heat and mass transfer processes as it definition is related to the ratio between the viscous and concentration boundary layers. Its effect on the species concentration has similar tendencies to the Prandtl number effect on the temperature. Then, an increase on the values of Sc causes the species concentration and its boundary layer thickness to decrease significantly as seen from figure 11.

Table 1. Steady-state values of $u'(t,x,0)$, $-T'(t,x,0)$ and $-C'(t,x,0)$ for various parametric conditions and $\boldsymbol{Gr=1}$, $\boldsymbol{Gc=2, \gamma=1}$ and $\mathrm{Re}=1$ and x=10.

Sc	Pr	t	γ	K	$u'(t,x,0)$	$-T'(t,x,0)$	$-C'(t,x,0)$
0.22	0.71	80	1	0.5	1.10948	0.0548108	0.2981304
0.60					0.9017683	0.0536343	0.3798349
0.94					0.8286249	0.0533622	0.4104386
0.62	0.9	200			0.8919809	0.0543561	0.3822405
	3				0.8414895	0.0803925	0.3823096
	5				0.8038385	0.1010115	0.382335
	100				0.4713726	0.32537	0.3823388
	0.71	10			0.7851977	0.1034868	0.3821992
		30			0.8758094	0.0621117	0.3822066
		50			0.8916470	0.0545334	0.3822288
		80			0.8935297	0.0536105	0.3822360
			0.5		0.8999031	0.0506627	0.3822115
			1		0.8959411	0.0524651	0.3822285
			5		0.8817145	0.0594307	0.3822601
			∞		0.872271	0.0642231	0.3822719
				0	2.8643805	0.0953962	0.3835340
				1	0.5320655	0.0506226	0.3822012
				2	0.2970914	0.0503607	0.3821977

Table 2. Steady-state values of $u'(t,x,0)$, $-T'(t,x,0)$ and $-C'(t,x,0)$ for various values of γ, Gr, Gc and Re and $Sc=0.62$, $\mathrm{Pr}=0.71$, $R=1$, $K=0.5$ and x=10.

γ	Gr	Gc	Re	$u'(t,x,0)$	$-T'(t,x,0)$	$-C'(t,x,0)$
1	1	2	1	0.8935297	0.0536105	0.3822360
			2	1.4492419	0.0813900	0.4268201
			3	1.8183454	0.1117785	0.4467778
			5	2.2182015	0.1607392	0.4655973
			10	2.4599510	0.2357999	0.4817568
	2	2	1	1.4775143	0.0627474	0.3823559
		4		1.7390950	0.0640959	0.3823807
		6		1.9996712	0.0655312	0.3824096
0	1	2		1.6993722	0.0685665	0.0884239
1				0.8935297	0.0536105	0.3822360
3				0.7435705	0.0531074	0.4464325
5				0.7018168	0.0530069	0.4651115

Figures 12-14 illustrate the transient state to steady-state conditions for the velocity, temperature and concentration profiles. It is seen that, from these figures, all of the velocity, temperature and concentration are increase as time progresses from the transient to the steady-state conditions. It is also seen that, the concentration profiles reach to the steady–state faster than the velocity and temperature profiles.

Figures 15-17 depict the typical velocity, temperature and concentration profiles for several values of the axial distance x. It is seen that all of the velocity, temperature and concentration increase as x increases.

The temporal developments of the skin-friction coefficient and the Nusselt number for various values of the Prandtl number are presented in figures 18 and 19. It is predicted that while the skin-friction coefficient increases with increasing time, the Nusselt number decreases as time progresses until they reach the steady state values. Also, it is clear that the skin-friction coefficient increases while the Nusselt number decreases as Pr increases.

Table 1 depicts the effects of parameters (K, Pr, R, and Sc) and dimensionless time t on the skin-friction coefficient [ ] and the rate of heat and mass transfer [and] for the fixed values , and x=10. It is observed from this table that the skin-friction coefficient increases as the thermal radiation parameter decreases while it decreases as either of the permeability parameter, Prandtl number and the Schmidt number increases. Moreover, the Nusselt number is increasing due to increases in the Prandtl number while it decreases as either of the permeability parameter, the inverse thermal radiation parameter (1/R) or the Schmidt number increases. In addition, the Sherwood number is increasing as a result of increasing the Schmidt number while it decreased as the permeability parameter increased.

Table 2 illustrates the skin-friction coefficient , rate of heat transfer and rate of mass transfer under the impacts of the thermal buoyancy (Grashof number) Gr, solutal

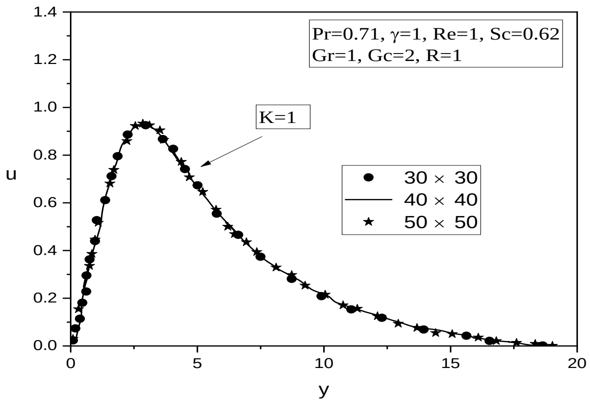

Figure 2. Grid independence results for the velocity profiles at (K=1, Pr=0.71, $Gr = 1, \quad Gc = 2, \gamma = 1, Sc = 0.62$and Re=1)

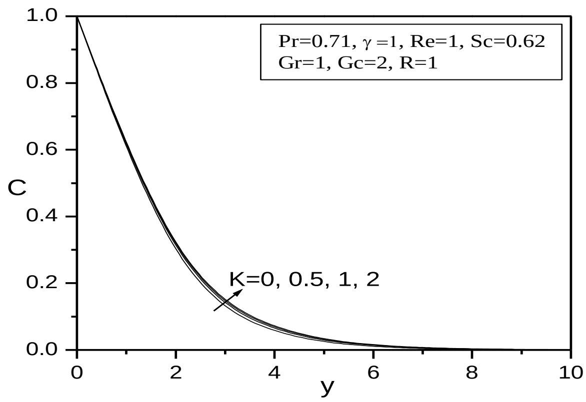

Figure 5. Effects of the permeability parameter on the concentration profiles

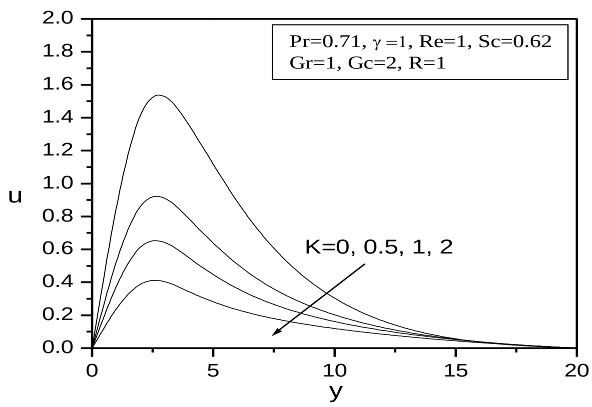

Figure 3. Effects of the permeability parameter on the velocity profiles

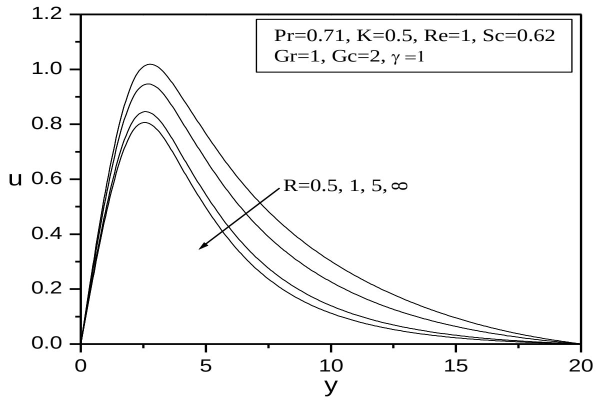

Figure 6. Effects of the radiation parameter on the velocity profiles

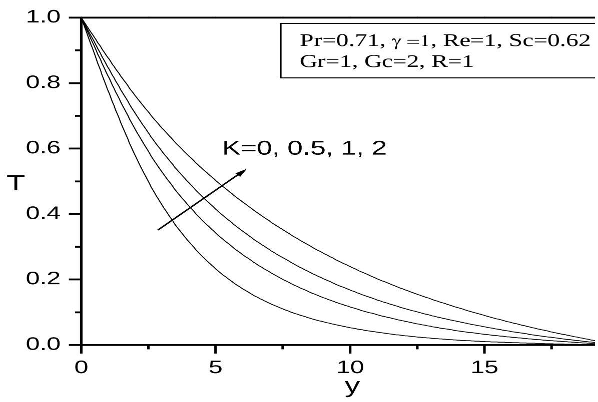

Figure 4. Effects of the permeability parameter on the temperature profiles

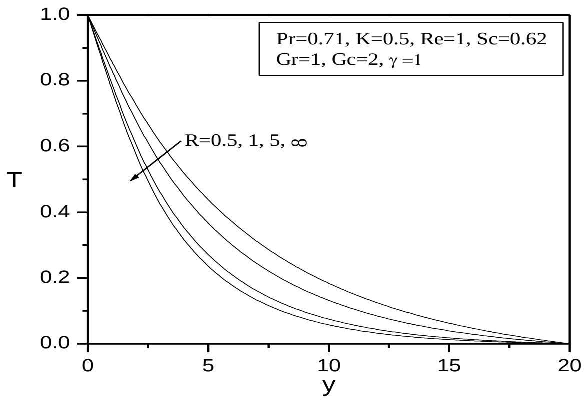

Figure 7. Effects of the radiation parameter on the temperature profiles

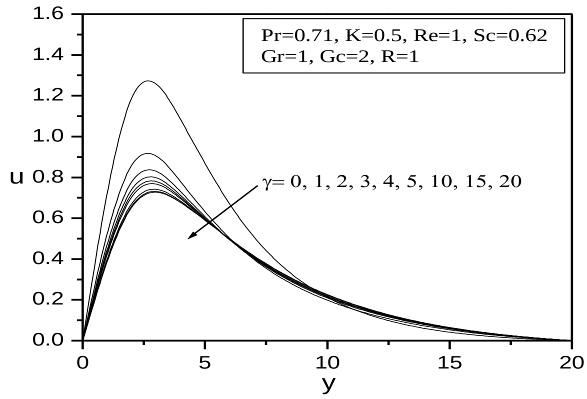

Figure 8. Effects of the chemical reaction parameter on the velocity profiles

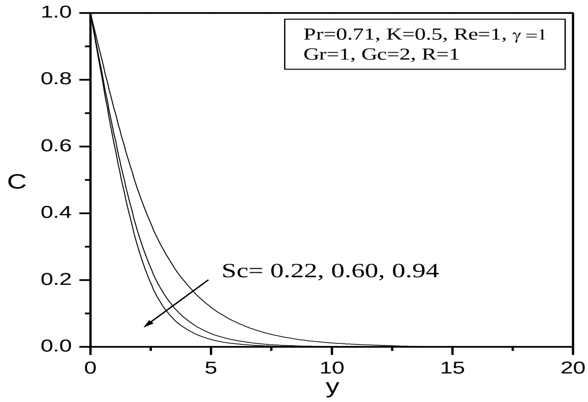

Figure 11. Effects of Schmidt number on the concentration profiles

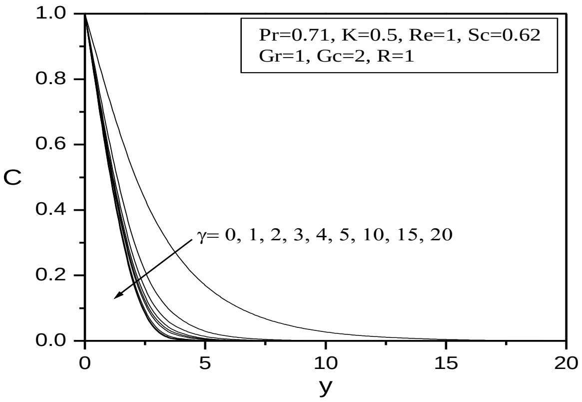

Figure 9. Effects of the chemical reaction parameter on the concentration profiles

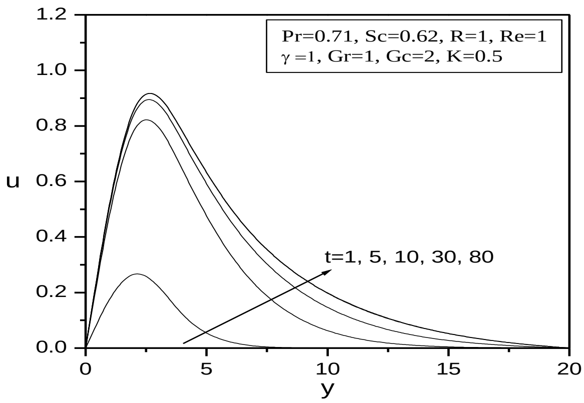

Figure 12. Development of velocity profiles with time

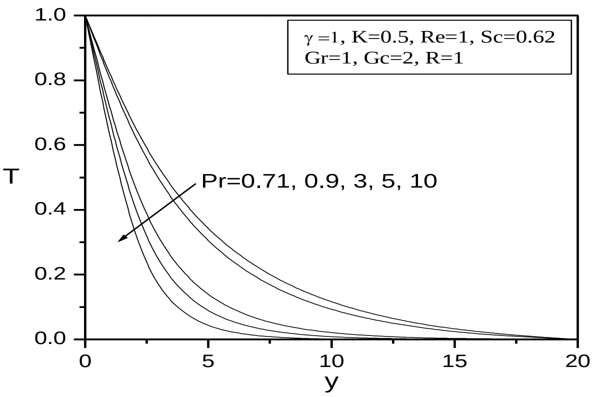

Figure 10. Effects of Prandtl number on the temperature profiles

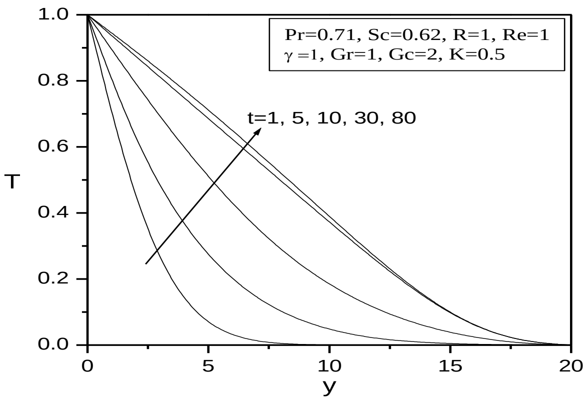

Figure 13. Development of temperature profiles with time

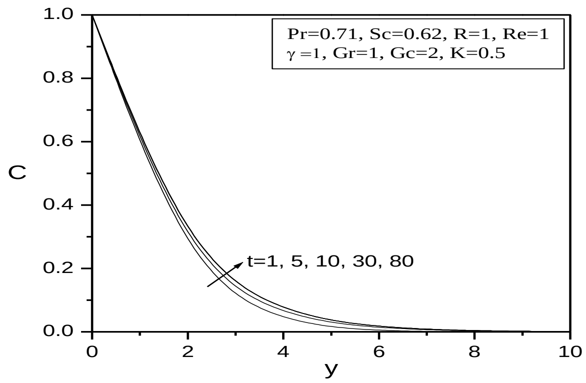

Figure 14. Development of concentration profiles with time

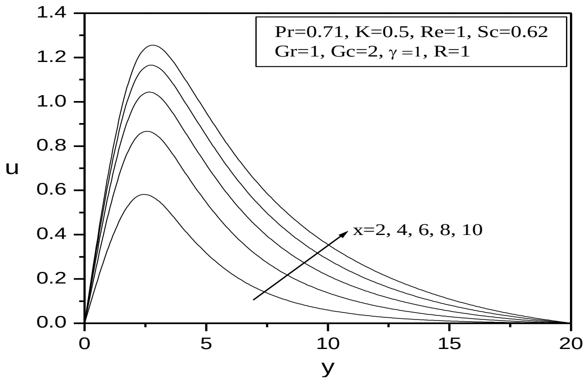

Figure 15. Velocity profiles for various values of *x*

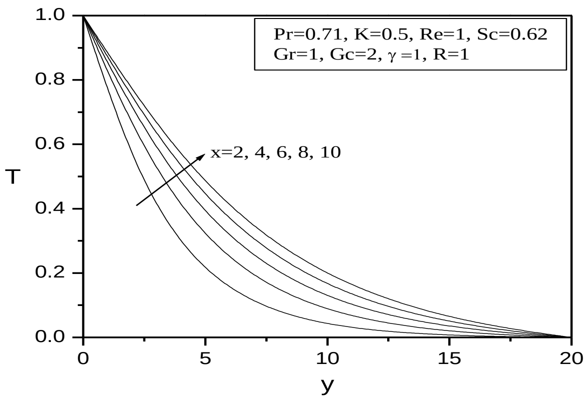

Figure 16. Temperature profiles for various values of *x*

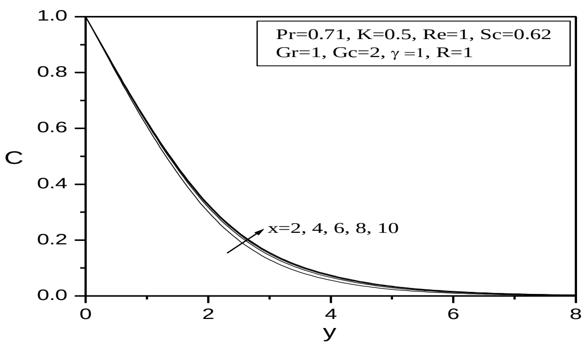

Figure 17. Concentration profiles for various values of *x*

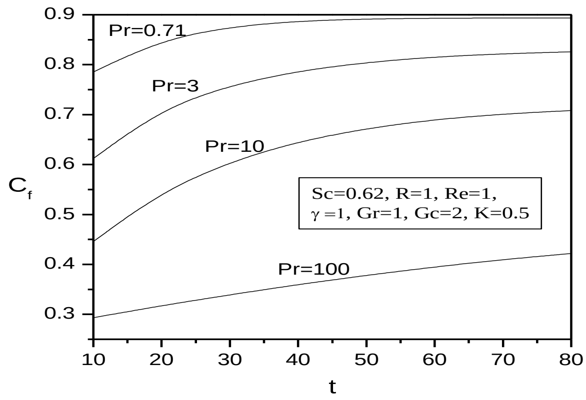

Figure 18. Temporal development of the skin-friction coefficient for various values of the Prandtl number

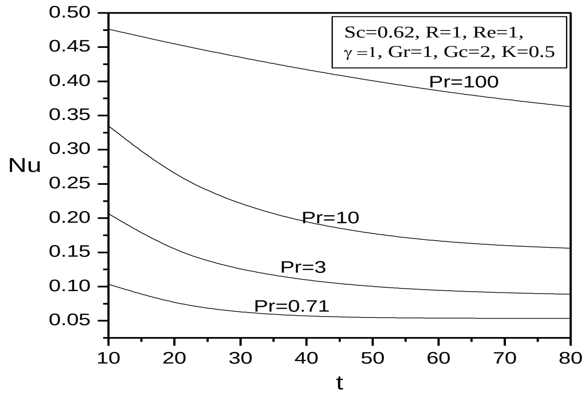

Figure 19. Temporal development of Nusselt number for various values of the Prandtl number

buoyancy (modified Grashof number) Gc, the Reynold number Re. Here, both the skin-friction coefficient and the the Nusselt number increase due to increases thermal buoyancy, solutal buoyancy or the Reynold number while they decrease as the chemical reaction parameter increases. The Sherwood number was predicted to increase as either of the thermal buoyancy, solutal buoyancy, Reynold number, or the chemical reaction parameter increases.

Conclusion

This work interest on the impacts of the chemical reaction and thermal radiation on natural convection boundary-layer flow of a viscous fluid over a vertical plate in a uniform porous medium. An explicit finite-difference scheme is used to solve the non-dimensionalized governing equations of this problem. Generally, the skin-friction coefficient increased as either of the thermal buoyancy, solutal buoyancy, Reynolds number or the inverse thermal radiation parameter increased and it decreased as a result of increasing either of the permeability parameter, Prandtl number, Schmidt number or the chemical reaction parameter. In addition, the Nusselt number increases due to increases in either of the Prandtl number, thermal buoyancy, solutal buoyancy or the Reynold number while it decreased as either of the permeability parameter, the inverse thermal radiation parameter, chemical reaction parameter or the Schmidt number increased. The Sherwood number increases as a result of increasing either of the thermal buoyancy, solute buoyancy, Reynold number, chemical reaction parameter or the Schmidt number while it decreased as the permeability parameter increased.

Nomenclature

C_p	specific heat
C	concentration
C_f	skin-friction coefficient
D_m	coefficient of mass diffusivity
G_c	modified Grashof number
Gr	Grashof number
K	permeability parameter
k	thermal conductivity
K_c	rate of chemical reaction
K^*	mean absorption coefficient
K_1	permeability of porous media
l	length of vertical plate
Nu	Nusselt number
Pr	Prandtl number
Sc	Schmidt number
Sh	Sherwood number
T	Temperature
q_r	radiative heat flux
t	time
R	radiation parameter
Re	Reynold's number
$\bar{x}, \bar{y}$	Cartesian coordinates
U	fluid velocity
$\bar{u}, \bar{v}$	velocity components

Greek symbols

β_T	volumetric coefficient of thermal expansion
β_c	volumetric coefficient of concentration expansion
ν	kinematic viscosity
μ	constant viscosity
ρ	fluid density
σ_0	Stefan-Boltzman constant
γ	chemical reaction parameter

Acknowledgements

The authors extend their appreciation to the Deanship of Scientific Research at King Khalid University, Abha, Saudi Arabia, for funding this work through the Research Group Project under Grant Number (RGP.1/19/42).

References

[1] M.Y. Gokhale, Magnetohydrodynamic transient-free convection past a semi-infinite vertical plate with constant heat flux, Can. J. Phys. 69 (1991) 1451–1453.

[2] H.S. Takhar, P. Ganesan, K. Ekambavahar, V.M. Soundalgekar, Transient free convection past a semi-infinite vertical plate with variable surface temperature, Int. J. Numer. Meth. Heat Fluid Flow 7 (1997) 280–296.

[3] R. Muthukumaraswamy, P. Ganesan, Unsteady flow past an impulsive by started vertical plate with heat and mass transfer, Heat Mass Transfer 34 (1998) 187–193.

[4] H.S. Takhar, R.S.R. Gorla, V.M. Soundalgekar, Radiation effects on MHD free convection flow of a gas past a semi-infinite vertical plate, Int. J. Numer. Meth. Heat Fluid Flow 6 (1996) 77–83.

[5] R. Muthucumaraswamy, P. Ganesan, Diffusion and first-order chemical reaction on impulsively started infinite vertical plate with variable temperature, Int. J. Therm. Sci. 41 (2002) 475–479.

[6] S.P. Anjali Devi, R. Kandasamy, Effects of chemical reaction, heat and mass transfer on non-linear MHD laminar boundary-layer flow over a wedge with suction or injection, Int. Commun. Heat Mass Transfer 29 (2002) 707–716.

[7] Sieniutycz Stanislaw, Nonlinear macrokinetics of heat and mass transfer and chemical or electrochemical reactions, Int. J. Heat Mass Transfer 47 (2004) 515–526.

[8] D. Abdulkadir, K. Yuksel, N. Veziroglu, Investigation of heat and mass transfer in a metal hydride bed, Applied Mathematics and Computation 150 (2004) 169–180.

[9] R. Kandasamy, K. Periasamy, K.K. Sivagnana Prabhu, Effects of chemical reaction, heat and mass transfer along a wedge with heat source and concentration in the presence of suction or injection, Int. J. Heat Mass Transfer 48 (2005) 1388–1394.

[10] R. Kandasamy, K. Periasamy, K.K. Sivagnana Prabhu, Chemical reaction, heat and mass transfer on MHD flow over a vertical stretching surface with heat source and thermal stratification effects, Int. J. Heat Mass Transfer 48 (2005) 4557–4561.

[11] A. J. Chamkha, A. M. Aly and M. A. Mansour, SIMILARITY SOLUTION FOR UNSTEADY HEAT AND MASS TRANSFER FROM A STRETCHING SURFACE EMBEDDED IN A POROUS MEDIUM WITH SUCTION/INJECTION and CHEMICAL REACTION EFFECTS, Chemical Engineering Communications,197:6, (2010) 846-858.

[12] A. J. Chamkha, A. M. Aly, and M. A. Mansour. "Unsteady natural convective power-law fluid flow past a vertical plate embedded in a non-Darcian porous medium in the presence of a homogeneous chemical reaction." Nonlinear Anal.: Model. Control 15.2 (2010): 139-154.

[13] A. J. Chamkha, M.A. Mansour, A. Aly, Unsteady MHD free convective heat and mass transfer from a vertical porous plate with Hall current, thermal radiation and chemical reaction effects, International Journal for Numerical Methods in Fluids, 65 (2011) 432-447.

[14] A. J. Chamkha and A. M. Aly, HEAT AND MASS TRANSFER IN STAGNATION-POINT FLOW OF A POLAR FLUID TOWARDS A STRETCHING SURFACE IN POROUS MEDIA IN THE PRESENCE OF SORET, DUFOUR AND CHEMICAL REACTION EFFECTS, Chemical Engineering Communications, 198: 2 (2010), 214-234.

[15] M.A. Mansour, N.F. El-Anssary, A.M. Aly, Effects of chemical reaction and thermal stratification on MHD free convective heat and mass transfer over a vertical stretching surface embedded in a porous media considering Soret and Dufour numbers, Chemical Engineering Journal, 145(2), (2008) 340-345.

[16] M.A. Abd El-Naby, E.M.E. Elbarbary, N.Y. Abed Elazem, Finite difference solution of radiation effects on MHD unsteady free-convection flow over vertical porous plate, Applied Mathematics and Computation 151 (2004) 327–346.

[17] P. Ganesan, G. Palani, Finite difference analysis of unsteady natural convection MHD flow past an inclined plate with variable surface heat and mass flux, Int. J. Heat Mass Transfer 47 (2004) 4449–4457.

[18] S.M.M. EL-Kabeir, A.M. Rashad, R.S.R. Gorla, Unsteady MHD combined convection over a moving vertical sheet in a fluid saturated porous medium with uniform surface heat flux, Mathematical and Computer Modelling 46 (2007) 384–397.

[19] I.U. Mbeledogu, A. Ogulu, Heat and mass transfer of an unsteady MHD natural convection flow of a rotating fluid past a vertical porous flat plate in the presence of radiative heat transfer, Int. J. Heat Mass Transfer 50 (2007) 1902–1908.

[15] E.M. Sparrow, R.D. Cess, Radiation heat transfer,Hemisphere, Augment Edition (1962).

[20] A.M. Rashad, M.M. Rashidi, G. Lorenzini, S.E. Ahme, A.M. Aly, Magnetic field and internal heat generation effects on the free convection in a rectangular cavity filled with a porous medium saturated with Cu–water nanofluid, International Journal of Heat and Mass Transfer, 104 (2017) 878-889.

[21] A. Basiri Parsa, M.M.Rashidi, O.Anwar Bég, S.M.Sadri, Semi-computational simulation of magneto-hemodynamic flow in a semi-porous channel using optimal homotopy and differential transform methods, Computers in Biology and Medicine, Vol. 43, Iss. 9 (2013) 1142-1153.

[22] Ali J. Chamkha, , M. F. El-Amin, and A. M. Aly. Unsteady double-diffusive natural convective MHD flow along a vertical cylinder in the presence of chemical reaction, thermal radiation and Soret and Dufour effects. Journal of Naval Architecture and Marine Engineering 8.1 (2011): 25-36.

[23] Ali J. Chamkha, A. M. Rashad, and Abdelraheem M. Aly. Transient natural convection flow of a nanofluid over a vertical cylinder, Meccanica 48.1 (2013): 71-81.

[24] Abdelraheem M. Aly, and Sameh Elsayed Ahmed. "Double-diffusive natural convective flow of a nanofluid over a vertical cylinder." Journal of Nanofluids 5.1 (2016): 110-119.